OPEN ACCESS Freely available online

PLoS GENETICS

Macoilin, a Conserved Nervous System–Specific ER Membrane Protein That Regulates Neuronal Excitability

Fausto Arellano-Carbajal[1☯¤a], Luis Briseño-Roa[1☯¤b*], Africa Couto[1], Benny H. H. Cheung[1], Michel Labouesse[2], Mario de Bono[1*]

1 Medical Research Council–Laboratory of Molecular Biology, Cambridge, United Kingdom, **2** Institute of Genetics and Molecular and Cellular Biology, Illkirch, France

Abstract

Genome sequence comparisons have highlighted many novel gene families that are conserved across animal phyla but whose biological function is unknown. Here, we functionally characterize a member of one such family, the macoilins. Macoilins are characterized by several highly conserved predicted transmembrane domains towards the N-terminus and by coiled-coil regions C-terminally. They are found throughout Eumetazoa but not in other organisms. Mutants for the single *Caenorhabditis elegans* macoilin, *maco-1*, exhibit a constellation of behavioral phenotypes, including defects in aggregation, O_2 responses, and swimming. MACO-1 protein is expressed broadly and specifically in the nervous system and localizes to the rough endoplasmic reticulum; it is excluded from dendrites and axons. Apart from subtle synapse defects, nervous system development appears wild-type in *maco-1* mutants. However, *maco-1* animals are resistant to the cholinesterase inhibitor aldicarb and sensitive to levamisole, suggesting pre-synaptic defects. Using *in vivo* imaging, we show that macoilin is required to evoke Ca^{2+} transients, at least in some neurons: in *maco-1* mutants the O_2-sensing neuron PQR is unable to generate a Ca^{2+} response to a rise in O_2. By genetically disrupting neurotransmission, we show that pre-synaptic input is not necessary for PQR to respond to O_2, indicating that the response is mediated by cell-intrinsic sensory transduction and amplification. Disrupting the sodium leak channels NCA-1/NCA-2, or the N-,P/Q,R-type voltage-gated Ca^{2+} channels, also fails to disrupt Ca^{2+} responses in the PQR cell body to O_2 stimuli. By contrast, mutations in *egl-19*, which encodes the only *Caenorhabditis elegans* L-type voltage-gated Ca^{2+} channel α1 subunit, recapitulate the Ca^{2+} response defect we see in *maco-1* mutants, although we do not see defects in localization of EGL-19. Together, our data suggest that macoilin acts in the ER to regulate assembly or traffic of ion channels or ion channel regulators.

Citation: Arellano-Carbajal F, Briseño-Roa L, Couto A, Cheung BHH, Labouesse M, et al. (2011) Macoilin, a Conserved Nervous System–Specific ER Membrane Protein That Regulates Neuronal Excitability. PLoS Genet 7(3): e1001341. doi:10.1371/journal.pgen.1001341

Editor: Andrew D. Chisholm, University of California San Diego, United States of America

Received June 3, 2010; **Accepted** February 16, 2011; **Published** March 17, 2011

Funding: This work was funded by the UK Medical Research Council. The funders had no role in study design, data collection and analysis, decision to publish, or preparation of the manuscript.

Competing Interests: The authors have declared that no competing interests exist.

* E-mail: debono@mrc-lmb.cam.ac.uk (MdB); briseno@biologie.ens.fr (LB-R)

☯ These authors contributed equally to this work.

¤a Current address: Facultad de Ciencias Naturales, Universidad Autónoma de Querétaro, Juriquilla, Querétaro, México
¤b Current address: INSERM U1024, École Normale Supérieure, Paris, France

Introduction

One of the most striking innovations in Metazoa is a nervous system with specialized nerve cells, pre- and post-synaptic structures, and associated signaling molecules. Neuronal signaling depends on complexes of multipass transmembrane proteins such as ion channels and G-protein-coupled receptors. Over the past few years several studies have identified specialized molecular machines in the endoplasmic reticulum by which particular complexes are assembled with appropriate stoichiometries and trafficked to their destination [1]. The emerging picture is that neurons have a highly specialized endoplasmic reticulum (ER), allowing channels to undergo quality control prior to export. However the identity of such maturation complexes remains unclear except for a handful of channels.

The extensive intracellular membrane system that makes up the ER varies, depending on cell type, but two domains, the rough and smooth ER (RER and SER), can usually be distinguished. The RER is studded with ribosomes and mediates translocation of secretory proteins across the membrane and insertion of membrane proteins. The SER is implicated in lipid synthesis and regulation of Ca^{2+} storage and signalling. Whereas most ER proteins are found in both RER and SER, a subset of proteins involved in translocation of newly synthesized proteins across the ER membrane is highly concentrated in the RER [2,3]. In *C. elegans* neurons, RER proteins are concentrated in the cell body and excluded from dendrites and axons, whereas general ER proteins are found in both cell body and neurites [4]. Electron microscopy confirms that ribosomes and RER are abundant in the cell body of *C. elegans* neurons but rare in neurites, whereas smooth ER-like structures can be seen in axons and dendrites as well as the cell body.

Over the last decade, genome sequencing projects have provided gene catalogs for animals representing a spectrum of metazoan phyla, including Placozoa [5], Cnidaria [6], Echinodermata [7], Annelida (http://genome.jgi-psf.org/Capca1/Capca1.home.html) and Chordata [8]. Genome-wide comparisons have identified human genes that are conserved across these

Author Summary

The human genome project has given us a catalog of the genes that make a human; however, the function of about 40% of these genes remains elusive. Many of these mysterious genes have relatives in simpler organisms like worms and flies, where their function can be studied much more easily than in a mammal. Here, we investigate one such family of genes, called macoilins, using the worm *C. elegans*. We show that worm macoilin, like mouse macoilin, is expressed widely but specifically in nerve cells. We create worms in which the macoilin gene is defective and show that, although they retain a nervous system that looks normal, they have behavioral defects. We show that these behavioral defects reflect an inability of nerves to signal efficiently. Nerve signalling relies on calcium channels and the defect of macoilin mutants resembles that of animals defective in a particular calcium channel component. We find that in nerve cells the macoilin protein resides specifically in the "factory" that assembles nerve signalling molecules, including calcium channels. Our results suggest that macoilin either directly helps assemble an ion channel or is needed to make a channel regulator. Our work in worms provides a blueprint to investigate the function of macoilins in mammals.

animal phyla, and highlighted their shared structural features. However the biological function of many of these conserved gene families remains mysterious. Genetic studies in model organisms such as *Drosophila* and *C. elegans* have provided a powerful way to functionally characterize novel conserved genes. This is exemplified by discovery of ion channel families, e.g. TRP [9], axon guidance pathways (UNC-6/netrin; UNC-40/DCC; ROBO [10]) and molecules involved in synaptic release (e.g. UNC-13 [11] and UNC-18 [12]). In all these cases genetic studies in flies or worms were recapitulated in mammals and catalyzed subsequent vertebrate work.

Here, we functionally characterize, for the first time, a member of a conserved family of proteins called macoilins. We find a macoilin gene in all available genome sequences of animals, from placozoa to man, but not in yeast or *Dictyostelium*. *C. elegans* macoilin, like mouse macoilin [13], is expressed throughout the nervous system. In *C. elegans* expression begins embryonically at the time neurons are born, and persists to adulthood. Using antibodies and compartment specific markers we show that *C. elegans* macoilin is localized to the rough endoplasmic reticulum and is excluded from neurites. We identify multiple *C. elegans* mutants of macoilin and show that these have altered behavior, but normal development of the nervous system. Using Ca^{2+} imaging, we show that macoilin is required for cell-intrinsic neuronal excitability in the O_2-sensing neuron PQR. This phenotype is mirrored in animals defective in EGL-19, the sole *C. elegans* L-type voltage gated ion channel (L-VGCC) alpha1 subunit. Our data suggest that macoilin is involved in assembly or traffic of ion channels or ion channel regulators.

Results

Mutations in *C. elegans* macoilin disrupt aggregation and are associated with multiple behavioral defects

N2, the laboratory wild-type strain of *C. elegans,* feeds in isolation; however most wild-collected strains of this species feed in groups [14–15]. N2 animals fail to aggregate because of a gain-of-function mutation in the neuropeptide receptor *npr-1*: if this receptor is knocked out they aggregate strongly [14][16]. To define genes that promote aggregation we mutagenized *npr-1(null)* animals and sought non-aggregating mutants. One complementation group we identified comprised three recessive alleles, *db1*, *db9* and *db129*, and defined a gene we called *maco-1* (for macoilin-1 see below). All three *maco-1* mutations strongly suppressed aggregation and bordering behaviors (Figure 1A) and disrupted the ability of *npr-1* animals to switch between roaming widely and dwelling locally according to ambient O_2 levels (Figure 1B) [17]. *maco-1; npr-1* mutants were healthy and displayed strong attraction to diacetyl and benzaldehyde (Figure S1A, S1B), odorants that are detected by the AWA and AWC olfactory neurons respectively [18]. They also strongly avoided high osmotic potential, a response mediated by ASH nociceptive neurons (Figure S1C) [19]. Like N2 animals, *maco-1* single mutants did not aggregate and only showed weak bordering behavior (Figure S1D). Closer examination, however, revealed additional behavioral phenotypes associated with *maco-1* mutations. We quantified these phenotypes in the presence of the N2 allele of *npr-1*, since this is the standard genetic background. First, harsh touch to the head elicited significantly longer reversals in *maco-1* mutants compared to N2 controls (Figure 1C). Second, *maco-1* mutants exhibited swimming defects [20] characterized by a decrease in the frequency of body bends (Figure 1D), an increase in the amplitude of body bends (data not shown), and coiling (Figure 1E). *maco-1* mutants also showed increased coiling when on an agar substrate (data not shown). Interestingly, the *maco-1* locomotory defects increased with age (Figure S1E, S1F). Third, whereas N2 animals suppress egg-laying in the absence of food [21], this inhibition was partly relieved in *db9* and *db129* mutant animals (Figure 1F). These subtle but pleiotropic defects of *maco-1* mutants suggest deficits in multiple neural circuits.

We mapped *maco-1* to a 30 kb interval on Chromosome I, close to D2092.5, a previously uncharacterized gene. DNA sequencing revealed that all three *maco-1* alleles disrupted D2092.5 (Figure 2A). The *db1* allele modified the splice donor site of intron 9 (G6024A); *db9* changed the arginine codon at position 534 to a stop codon and is predicted to truncate the MACO-1 protein (Figure 2D); the *db129* allele was associated with a mutation in the splice acceptor site of intron 2 (G595A). Together, these data suggest that *maco-1* corresponds to D2092.5. This was confirmed by transgenic rescue of the *maco-1* mutant phenotypes with a wild-type D2092.5 transgene (Figure S2A–S2D). None of our *maco-1* alleles were unambiguously null mutants. However the premature stop codon associated with the *db9* allele would be expected to cause nonsense mediated degradation of *maco-1* mRNA, as well as truncating half the MACO-1 protein, and therefore to be a strong loss-of-function mutation. Consistent with this, the phenotypes of *maco-1(db9)/maco-1(db9)* and *maco-1(db9)/qDf16* were similar (Figure S1G); *qDf16* is a large deletion that spans the *maco-1* interval (see Materials and Methods).

cDNA analyses indicated that the D2092.5 gene can encode two splice isoforms by alternate splicing at exon 5 (Figure 2A). The proteins encoded by the resulting mRNAs were 908 (MACO-1a) and 897 (MACO-1b) amino acids long. Blast searches identified these proteins as homologues of vertebrate macoilins. Reciprocally, searching the *C. elegans* genome with vertebrate macoilins identified only one homologue, D2092.5 (Figure 2D). At least one macoilin can be found in every animal genome sequenced so far (Figure 2B, 2C). In some fish lineages but not in other vertebrates, a second MACO homologue can be found (MACO-2); MACO-2 probably arose during the genome duplication event that is thought to have occurred in teleost fish. Despite this ubiquity, little

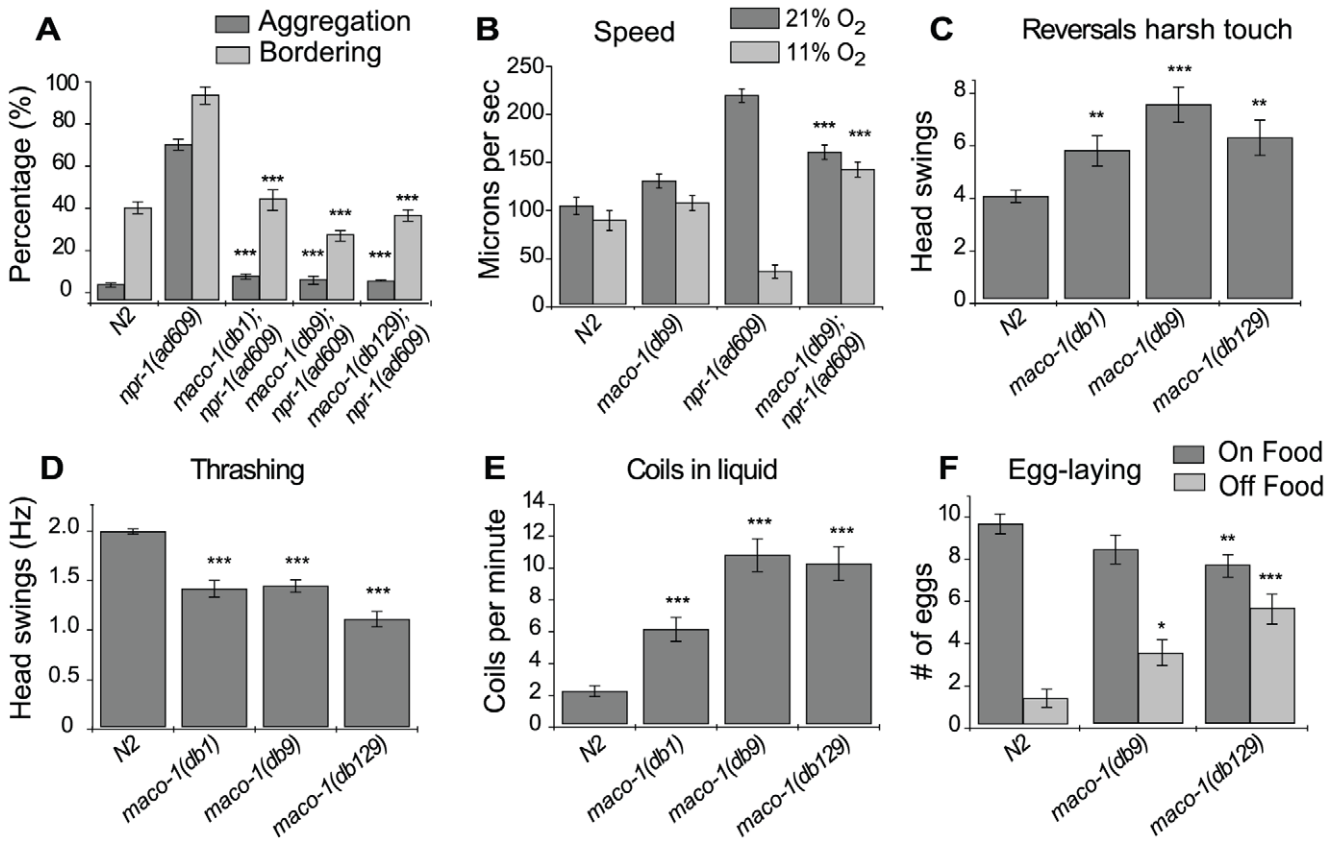

Figure 1. *maco-1* mutants exhibit multiple behavioral defects. (A, B) *npr-1(ad609)* animals aggregate, accumulate on the border of a bacterial lawn, and roam widely in high (21%) ambient O_2 but dwell locally in low (11%) O_2. *maco-1* mutations disrupt these behaviors. (C) *maco-1* animals reverse more than wild type in response to a harsh prod to the head (n = 30; *t*-test). (D, E) *maco-1* mutants have swimming defects, with a loss of head swings and increased coiling (n = 15; *t*-test); (F) *maco-1* mutants fail to appropriately suppress egg laying when food is absent (n = 22–29 animals; K-S-test). * equals $p<0.05$; ** equals $p<0.01$; *** equals $p<0.001$. Error bars indicate s.e.m.
doi:10.1371/journal.pgen.1001341.g001

is known about this protein family. The only macoilin previously investigated is the mouse homologue, highlighted because it is expressed differentially between wild-type mice and *reeler* mutants [22],[13]. *In situ* hybridization indicates that mouse macoilin mRNA is highly expressed in all neuronal differentiation fields from embryonic stage E12.5 to birth [13]. After birth (PG10), expression decreases but remains associated with some neurons such as cerebellar granule cells, olfactory mitral and granule cells, pyramidal neurons in the hippocampus, and granule cells in dentate gyrus [13]. No significant expression of mouse macoilin has been reported outside the nervous system.

Comparison of macoilin sequences across phyla highlighted several common features (Figure 2D). All MACO-1 homologs were predicted to have at least three transmembrane domains towards the N-terminus and at least two coiled-coil domains towards the C-terminus. The exact number of transmembrane and coiled-coil domains varied depending on the prediction algorithm and species (data not shown). At the sequence level the transmembrane and coiled-coil domains were the most conserved parts of the protein (Figure 2D).

C. elegans macoilin is a pan-neuronally expressed ER protein

To determine where *maco-1* was expressed, we created transgenic *C. elegans* that co-expressed *maco-1* and *gfp* coding sequences as a polycistronic message from the *maco-1* promoter. These animals first showed GFP fluorescence 6 hours after the first cell division (Figure S3A). By late embryogenesis and in the L1 larva, fluorescence was visible throughout the nervous system (Figure S3A). In adults, the GFP signal remained pan-neuronal, with very occasional expression in other tissues (Figure S3B). Thus, *C. elegans* MACO-1, like its mouse homologue, is expressed widely and almost exclusively in the nervous system.

To study endogenous MACO-1, we raised polyclonal antibodies against the C-terminus of both its protein isoforms. N2 worms stained with the antibody showed bright expression in most or all *C. elegans* neurons (Figure 3A–3C and Figure S4A). In contrast, *maco-1(db9)* mutants which have a nonsense mutation that truncates MACO-1 upstream of the epitope sequence showed no signal in the nervous system (Figure 3D, 3E, and Figure S4B, S4C). Interestingly, MACO-1 antibody staining was restricted to the neuronal cell body: no staining was observed in dendrites, in the synapse-rich axon bundles that make up the nerve ring, or in the axons comprising the ventral and dorsal cords (Figure 3A, 3B). To confirm that MACO-1 was absent from synapses, we co-stained worms expressing the synaptic marker SNB-1-GFP in GABAergic neurons (*juIs1*) with anti-MACO-1 and anti-GFP antibodies: the two markers did not show co-localization (Figure 4A–4D). Moreover, worms co-expressing *juIs1* and *psnb-1::maco-1-mcherry* showed that transgenic MACO-1-cherry was also restricted to the cell body of neurons, overlapping only with the SNB-1-GFP signal in the cell body of GABAergic neurons

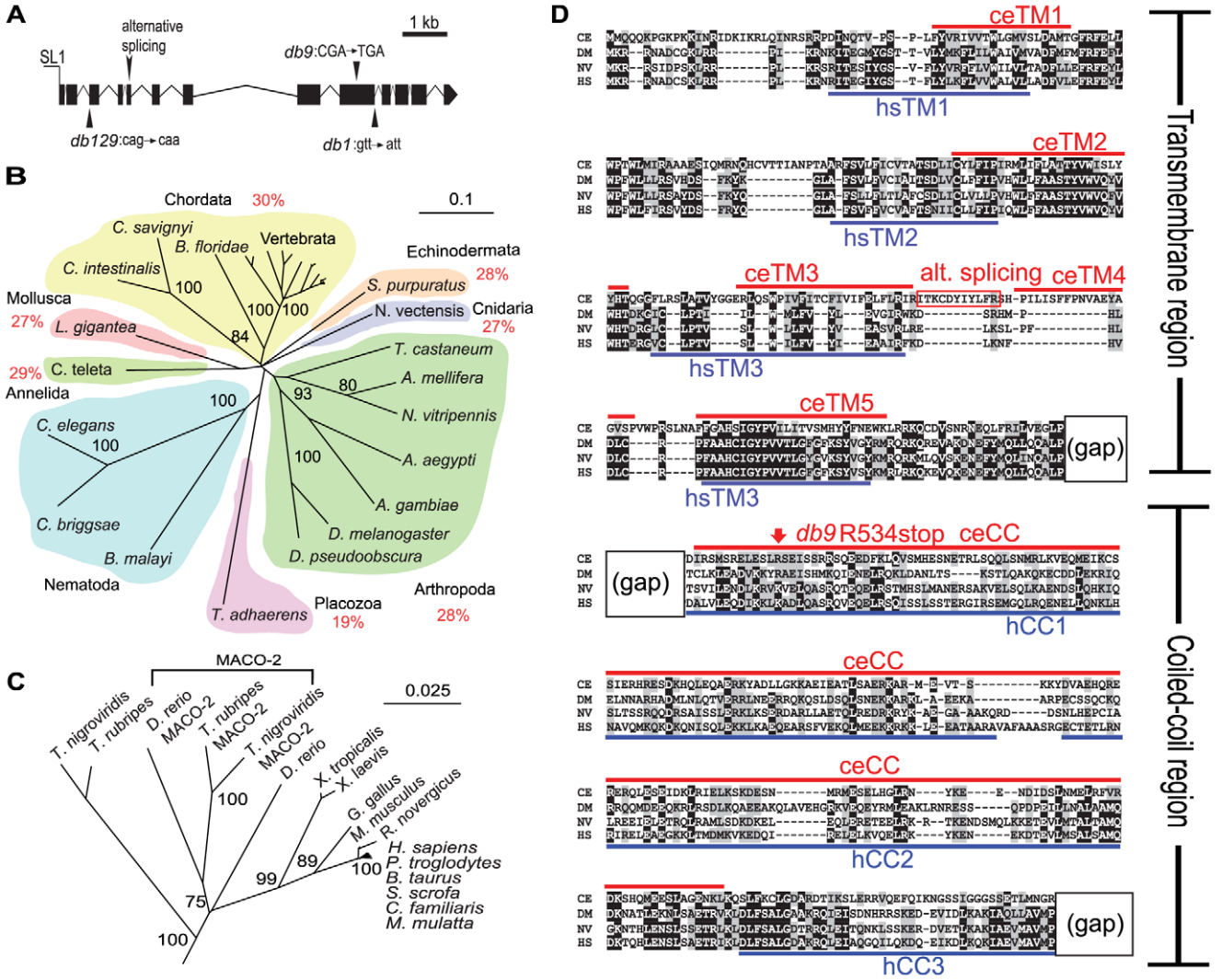

Figure 2. ***maco-1*** **mutations disrupt macoilin, a polytopic membrane protein with coiled-coil domains that is conserved across Eumetazoa.** (A) *maco-1* mutations disrupt D2092.5 which encodes *C. elegans* macoilin. Arrows indicate locations of the three *maco-1* alleles; also indicated is the alternative splicing site. (B–C) Unrooted Neighbor-Joining tree of MACO-1 homologues and 10000 bootstrap replicates analysis and scale bar denoting 0.10 and 0.25 changes per site in (B) and (C), respectively. (B) Branches are grouped by phyla with colored lobes; the average sequence identity with MACO-1 is shown in percentile figures. (C) Zoom-in of the tree of the vertebrate sub-phyla. MACO-2 is a second macoilin gene found in some fish lineages but not in other vertebrates (see text). (D) Multiple alignments of MACO-1 homologues. Predicted transmembrane (TM) and coiled-coil (CC) domains in *C. elegans* and *H. sapiens* are shown in red and blue respectively. CE, *C. elegans*; DM, *D. melanogaster*; NV, *N. vectensis*; TR; HS, *H. sapiens*. A more extensive alignment can be found in Figure S10.
doi:10.1371/journal.pgen.1001341.g002

(Figure 4N). Both transgenic and endogenous MACO-1 was also found restricted to neuronal cell bodies at embryonic developmental stages (Figure S5).

The striking localization of MACO-1 to the cell body raised the possibility that it resides in a specific membrane compartment. To investigate this we created different transgenic lines that expressed organelle-specific markers in a subset of neurons, using the *glr-1* promoter (*glr* = glutamate receptor) (Figure 4E–4M; Figure S6). The markers used (a kind gift of M. M. Rolls, Pennsylvania State University) were phosphatidylinositol synthase (PIS) for the general endoplasmic reticulum (ER), translocating chain-associating membrane protein (TRAM) for rough ER, Emerin for the nuclear envelope, and Mannosidase (MANS) for the Golgi. All markers were tagged at the N-terminus with YFP. Co-immunostaining of MACO-1 and YFP revealed partial co-localization between MACO-1 and the ER general marker, YFP-PIS (Figure 4E–4I). Within the ER, MACO-1 was further co-localized with a marker restricted to the rough ER, YFP-TRAM, and nuclear envelope, YFP-Emerin (Figure 4J-4M and Figure S6A–S6D). Similar ER localization was seen in embryonic stages (Figure S6). No significant co-localization was observed with the Golgi-specific marker, YFP-MANS (Figure S6E–S6H; however the cell bodies of *C. elegans* neurons are small (2 microns), making it difficult to exclude the possibility that there is a low amount of MACO-1 in Golgi. These co-localization experiments suggest that MACO-1 predominantly resides in the ER of neurons, in particular in rough ER and nuclear envelope. We observed no gross morphological defects in *maco-1* worms in any of the subcellular compartments expressing the YFP tagged constructs described above (data not shown).

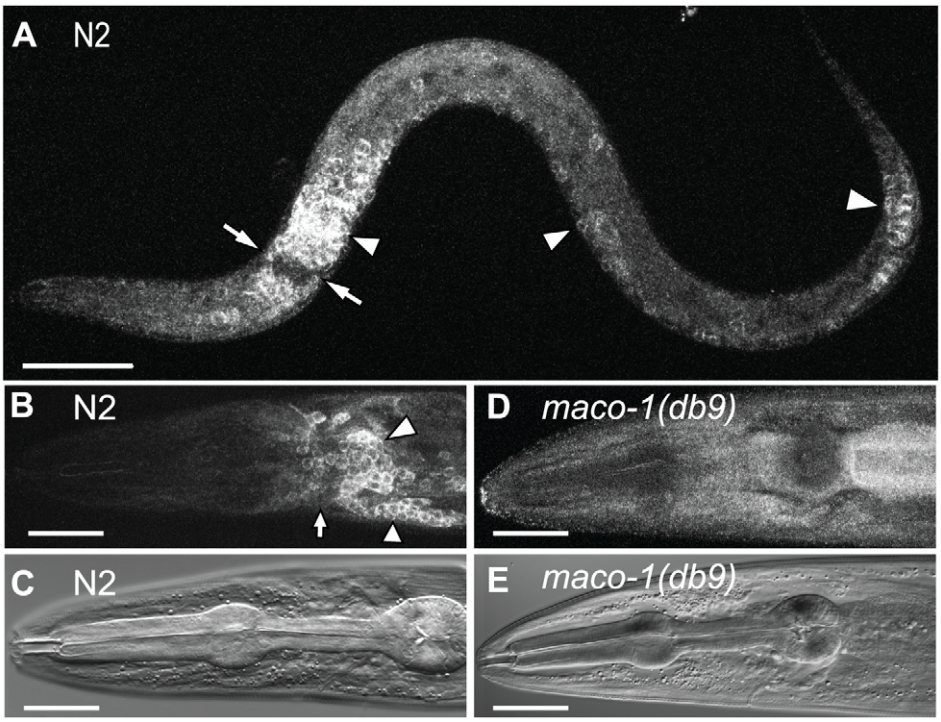

Figure 3. Endogenous MACO-1 is localised to the cell body of neurons. Immunohistochemical staining of N2 larvae (A) and of N2 and *maco-1* adult worms (B–E) using affinity purified anti-MACO-1 antibodies. Arrowheads indicate staining in neuronal cell bodies. A, B and D show fluorescence images whereas C and E show DIC images. Arrows indicate absence of staining in the nerve ring. *maco-1(db9)* mutants, which bear a premature stop codon truncating MACO-1 before the epitope recognised by the anti-MACO-1 antibodies, exhibit no neuronal staining (see also Figure S4). Scale bars represent 20 μm.
doi:10.1371/journal.pgen.1001341.g003

C. elegans macoilin mutants have wild-type neuronal cell morphology, axon guidance, and axon polarity

The broad neuronal expression patterns of *C. elegans* and mouse macoilins suggest that this protein family has a general role in the development or function of the nervous system. To elucidate this role, we first examined the anatomy of the nervous system in *maco-1(db9)* mutants using neuron-specific GFP reporters. We examined mechanosensory neurons, chemosensory neurons, and GABAergic motor neurons. We detected no overt abnormalities in the cell bodies, axons, dendrites or cilia of any neuron we examined (Figure S7A–S7C and data not shown). We next asked if *maco-1* regulates neuronal polarity (i.e. the placement of synapses) or axonal trafficking of synaptic vesicles. To test this we visualized synaptic vesicles in live animals using a fluorescently-tagged synaptic vesicle marker, synaptobrevin-GFP (SNB-1::GFP). We saw no defects either in the GABAergic DD motor neurons or in the URX O_2-sensing neurons (Figure S7D–S7G and data not shown). These results suggest that MACO-1 is not required for correct establishment or maintenance of neuron polarity.

Precursor vesicles containing synaptic proteins are generated at the cell body and transported to synapses by microtubule-based motor proteins [23]. In *C. elegans*, this transport requires the KIF1A kinesin homologue *unc-104* [23]. In *unc-104* mutants tagged synaptobrevin expressed from the *punc-25::snb-1::gfp* transgene is retained in the cell bodies of the DD and VD motor neurons [24]. Macoilins have been proposed to function in axonal traffic [13]; however, in adult *maco-1(db9)* worms expressing the *punc-25::SNB-1::GFP* marker, the tagged synaptobrevin was still localized along the ventral and dorsal nerve cords (Figure 6A and 6C). This suggests that MACO-1 is not essential for transport of synaptic vesicles.

maco-1 mutants are resistant to aldicarb but sensitive to levamisole

C. elegans synaptic function can be assayed by studying responses to the acetylcholinesterase inhibitor aldicarb and the acetylcholine receptor agonist levamisole [20,25]. Aldicarb inhibits acetylcholinesterase (AChE), leading to accumulation of acetylcholine at the neuromuscular junction (NMJ), overstimulation of acetylcholine receptors, and paralysis of wild-type animals. Mutants defective in synaptic release have reduced acetylcholine accumulation and are therefore resistant to aldicarb [20]. However these mutants retain sensitivity to levamisole, which directly activates post-synaptic acetylcholine receptors. In contrast, mutants defective in postsynaptic responses to ACh are resistant to both aldicarb and levamisole [26]. *maco-1(db9)* mutants were resistant to aldicarb but sensitive to levamisole (Figure 5A, 5B), suggesting they have presynaptic defects in neurotransmission.

maco-1 mutants show subtle synapse morphology defects

The aldicarb resistance of *maco-1* mutants prompted us to examine synapse structure in these animals more closely. GABAergic type D motor neurons form neuromuscular junctions (NMJs) with ventral and dorsal body wall muscles [27]. We visualized the presynaptic terminals of these neurons using the *punc-25::snb-1::gfp* transgene *juIs1* [28]. Wild-type animals bearing *juIs1* have SNB-1::GFP puncta of uniform shape and size distributed evenly along the ventral and dorsal nerve cord. These puncta correspond to the presynaptic termini of the 13 VD and 6 DD neurons, respectively. We measured puncta size and number along a 100 μm section of the ventral nerve cord (Figure 6). In

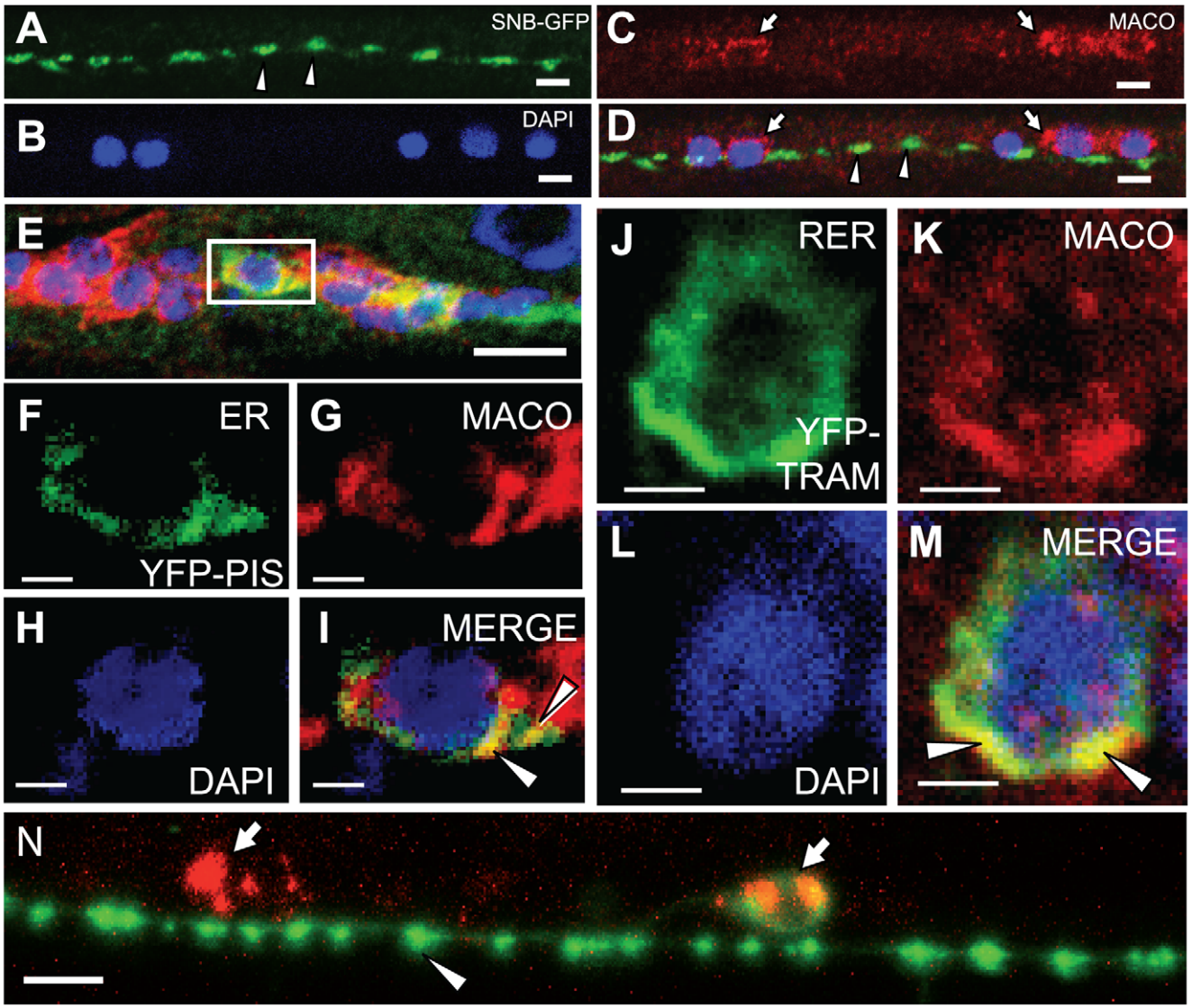

Figure 4. MACO-1 resides in the endoplasmic reticulum (ER). Confocal optical sections of neurons in *C. elegans* co-stained with anti-MACO-1 and anti-GFP antibodies and expressing different markers: (A–D) the synaptic marker synaptobrevin-1-GFP (*juIs1*) (SNB-GFP); (E–I) an extrachromosomal array expressing the general ER marker YFP-Phosphatidylinositol synthase (YFP-PIS); (J–M) an extrachromosomal array expressing the rough ER marker Translocating chain-associating membrane protein (YFP-TRAM). Staining: A, F, J, anti-GFP antibodies; B, H, L, DAPI; C, G, K, anti-macoilin antibody. Neurons correspond to (A–D) the ventral cord motor-neurons between the gonad posterior reflex and the pre-anal ganglia, (F–I) the retrovesicular ganglia and (J–M) head. In C and D arrows indicate MACO-1 signal in the neuronal cell bodies and arrowheads indicate synapses. In I and M arrowheads indicate co-localisation between the MACO-1 and the ER markers PIS and TRAM. Scale bars represent **(**A–D) 2, (E) 5 and (F–M) 1 μm. N. MACO-1-mCherry fails to localize to synapses. Shown is a merge of green and red fluorescence for a section of the ventral cord from animals that express *psnb-1::maco-1-mcherry* (*psnb-1* drives expression in all neurons) and *juIs1*, *punc-25::snb-1-GFP*. The arrows indicate cell bodies; arrowheads indicate synapses. Scale bar is 5 μm.
doi:10.1371/journal.pgen.1001341.g004

wild-type animals, average puncta area in the ventral nerve cord was 1.58 ± 0.13 μm^2, with an average of 23.28 ± 0.79 puncta per 100 μm ($n=22$ animals). *maco-1* mutants had fewer puncta that tended to be larger: the average size in the ventral nerve cord was 2.62 ± 0.54 μm^2 with an average of 19.87 ± 1.18 μm puncta per 100 μm ($n=23$) (Figure 6A–6D). These data suggest that *maco-1* influences pre-synaptic structure.

We next investigated whether *maco-1* mutants exhibit active zone defects, using SYD-2::GFP [29] and UNC-10::GFP [30] as markers (Figure 6E–6L). Both fusion proteins were expressed in the GABAergic VD and DD motorneurones from the *unc-25* promoter. Wild-type animals carrying the *punc-25::syd-2::gfp* transgene *hpIs3* have regularly-sized and spaced puncta along the dorsal and ventral nerve cords, with an average punctal area of 0.32 ± 0.017 μm^2 and on average 36.78 ± 1.96 ($n=17$) puncta per 100 μm. In *maco-1(db9)* adult animals the number of SYD-2::GFP puncta along the dorsal nerve cord was increased but their size was similar to wild-type (Figure 6I–6L). The average area of puncta in *maco-1* mutants was 0.31 ± 0.014 μm^2, with an average of 45.44 ± 1.51 ($n=23$) puncta per 100 μm. Wild-type animals carrying the *punc-25::unc-10::gfp* transgene *hpIs61* have uniformly shaped and evenly distributed puncta along the ventral and dorsal cord. In *maco-1(db9)* adult animals, there was a reduced number of puncta but they were larger than in wild-type animals in the

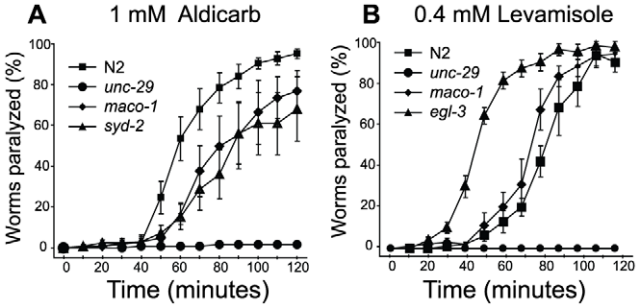

Figure 5. *maco-1* mutants are resistant to aldicarb but sensitive to levamisole. (A) *maco-1(db9)* animals are resistant to aldicarb but (B) sensitive to levamisole, consistent with a pre-synaptic role for MACO-1. Also plotted are control responses of N2 animals and mutants in the nicotinic acetylcholine receptor subunit *unc-29(e193)* and the synapse defective gene *syd-2(ju37),* which encodes alpha liprin.
doi:10.1371/journal.pgen.1001341.g005

ventral nerve cord. The average punctum area in the ventral nerve cord for wild-type animals was 0.55 ± 0.035 μm^2, with an average of 35.16 ± 0.99 (n = 13) puncta per 100 μm. Average puncta size in *maco-1* mutants was 0.85 ± 0.12 μm^2, and the average number of puncta was 28.12 ± 2.29 (n = 12) per 100 μm (Figure 6E–6H). Together these data suggest that loss of *maco-1* alters the structure of the synaptic active zone, but the effects are subtle.

We also examined the periactive zone, using the marker RPM-1::GFP [31]. This region just surrounds active zones and has been proposed to regulate synapse growth [32]. We found a slight increase in the size and number of puncta in *maco-1* mutants (0.75 ± 0.068 μm^2 and 37.24 ± 3.376, n = 10), compared to wild-type animals (0.63 ± 0.036 μm^2 and 33.09 ± 2.7, n = 16). However, these differences were not significant (p = 0.1 and p = 0.34, respectively), suggesting that the periactive zone was not disorganized in *maco-1* mutants.

maco-1 mutants have defects in Ca^{2+} influx

Synapse development can be influenced by neural activity [33]. This prompted us to explore if the subtle synaptic defects in *maco-1* reflected altered neuronal excitability. We focused our analyses on the O_2-sensing neuron PQR, since a subset of the phenotypes of *maco-1* mutants resembled those associated with loss of O_2 sensing neurons [34]. To image Ca^{2+} transients we used the cameleon reporter YC3.60 [35] expressed from the *gcy-32* promoter [15]. Baseline Ca^{2+} levels in 7% O_2 were similar in wild type and *maco-1* mutants, suggesting that PQR neurons were not chronically depolarized in *maco-1* mutants. However the Ca^{2+} rise seen in wild type when O_2 is raised to 21% was absent in most *maco-1* mutant animals (Figure 7A). These data suggest that *maco-1* is required for efficient activation of PQR neurons in response to a rise in O_2.

To explore this further we first asked if pre-synaptic input was required for PQR neurons to respond to O_2 stimuli. Null mutations in *unc-13* or *unc-31* CAPS, which disrupt release of synaptic vesicles and dense core vesicles respectively, did not significantly alter Ca^{2+} transients in PQR to a 7 – 21% O_2 upstep or a 21 to 7% downstep (data not shown). This suggests that Ca^{2+} fluxes in PQR reflect cell-intrinsic responses to the O_2 stimuli, and that loss of *maco-1* disrupts either primary sensory transduction of ambient O_2 or amplification of the sensory potential. O_2-stimulated Ca^{2+} influx in PQR requires the atypical soluble guanylate cyclases GCY-35 and GCY-36. These soluble guanylate cyclases are themselves O_2 sensors and activate a cGMP-gated ion channel [36-37]. Consistent with this, in a separate study we have shown that a rise in O_2 stimulates a rise in cGMP in PQR neurons (A.C. and M.dB, in preparation). Mutations in *maco-1* did not alter PQR cGMP responses to an O_2 stimulus, suggesting that O_2 sensing by GCY-35/36 was unaffected (A.C. and M.dB, in preparation).

Previous work has shown that *tax-4*, which encodes a cGMP-gated cation channel alpha subunit is required for the O_2-evoked Ca^{2+} transients in PQR [15]. To explore how depolarization evoked by the cGMP channel is amplified and leads to Ca^{2+} influx in the cell body we imaged PQR responses to O_2 stimuli in animals defective in various ion channels. The *C. elegans* genome does not appear to encode voltage-gated sodium channels. Instead, electrical signals are thought to propagate via voltage-gated Ca^{2+} channels and cation leak channels [38,39]. *C. elegans* encodes 3 voltage gated Ca^{2+} channel α1 subunits: *egl-19* (CaV1, L-type), *unc-2* (CaV2, N-, P/Q, R-type) and *cca-1* (CaV3, T-type) [40]. It also encodes 2 homologs of the vertebrate cation leak channel NALCN that regulates neuronal excitability [38]. Animals mutant for the UNC-2 P/Q-like voltage-gated Ca^{2+} channel (VGCC) [41], the T-type channel CCA-1 [42], or double mutant for the NCA-1and NCA-2 NALCN-like leak channels [38] showed overtly wild-type Ca^{2+} transients in the cell body of PQR in response to a 7 to 21% O_2 shift (Figure 7C and data not shown). This is consistent with previous results in other neurons that suggest these channels contribute to Ca^{2+} signals at synapses and axons, but are not essential for Ca^{2+} changes in the cell body [38,39]. In contrast, animals with partial loss-of-function mutations in the EGL-19 L-type VGCC showed frequent failure of cell body Ca^{2+} transients (Figure 7B). L-type VGCCs have previously been shown to contribute to dendritic Ca^{2+} currents both in *C. elegans* [39] and vertebrates [43]. Consistent with these imaging results, *egl-19(ad1006); npr-1(ad609)* double mutants animals failed to aggregate.

Together, our Ca^{2+} imaging results suggest that MACO-1 acts in the endoplasmic reticulum to promote assembly and/or traffic of either a cGMP-gated cation channel that contains the TAX-4 alpha subunit, or of an L-type Ca^{2+} channel containing the EGL-19 α1 subunit, or of another as yet unknown regulator that modulates O_2-evoked Ca^{2+} entry into PQR. To investigate the first possibility we made transgenic animals that expressed a functional GFP-tagged TAX-4 protein in the AQR, PQR and URX neurons, and compared the localization of this channel subunit in *npr-1* and *maco-1; npr-1* mutant animals. We saw enrichment of TAX-4-GFP in the sensory endings of the O_2-sensing neurons, as expected for a sensory transduction channel (Figure S8). We also observed TAX-4-GFP in the cell body and on axons and dendrites. However we found no effect of loss-of-function mutations in *maco-1* on this distribution pattern (Figure S8 and data not shown). These data suggest *maco-1* is not required for TAX-4 to be exported from the ER, although they do not rule out a potential role in the function of a TAX-4-containing channel. Next, we transgenically expressed EGL-19 protein that is N-terminally tagged with GFP from its endogenous promoter, and examined its localization in wild type and *maco-1* mutant animals. As expected, GFP-EGL-19 was expressed very broadly, and both in muscles and neurons (Figure S9) [44]. In neurons GFP-EGL-19 was enriched in sensory endings and in cell bodies. However we did not see any striking defects in the EGL-19 localization pattern in *maco-1* mutants (Figure S9). This does not rule out that MACO-1 modulates the function of an EGL-19-containing channel, but it does suggest that if it has a role it involves only a subset of EGL-19-containing channels; alternatively *maco-1* regulates function of other, as yet unknown, ion channels.

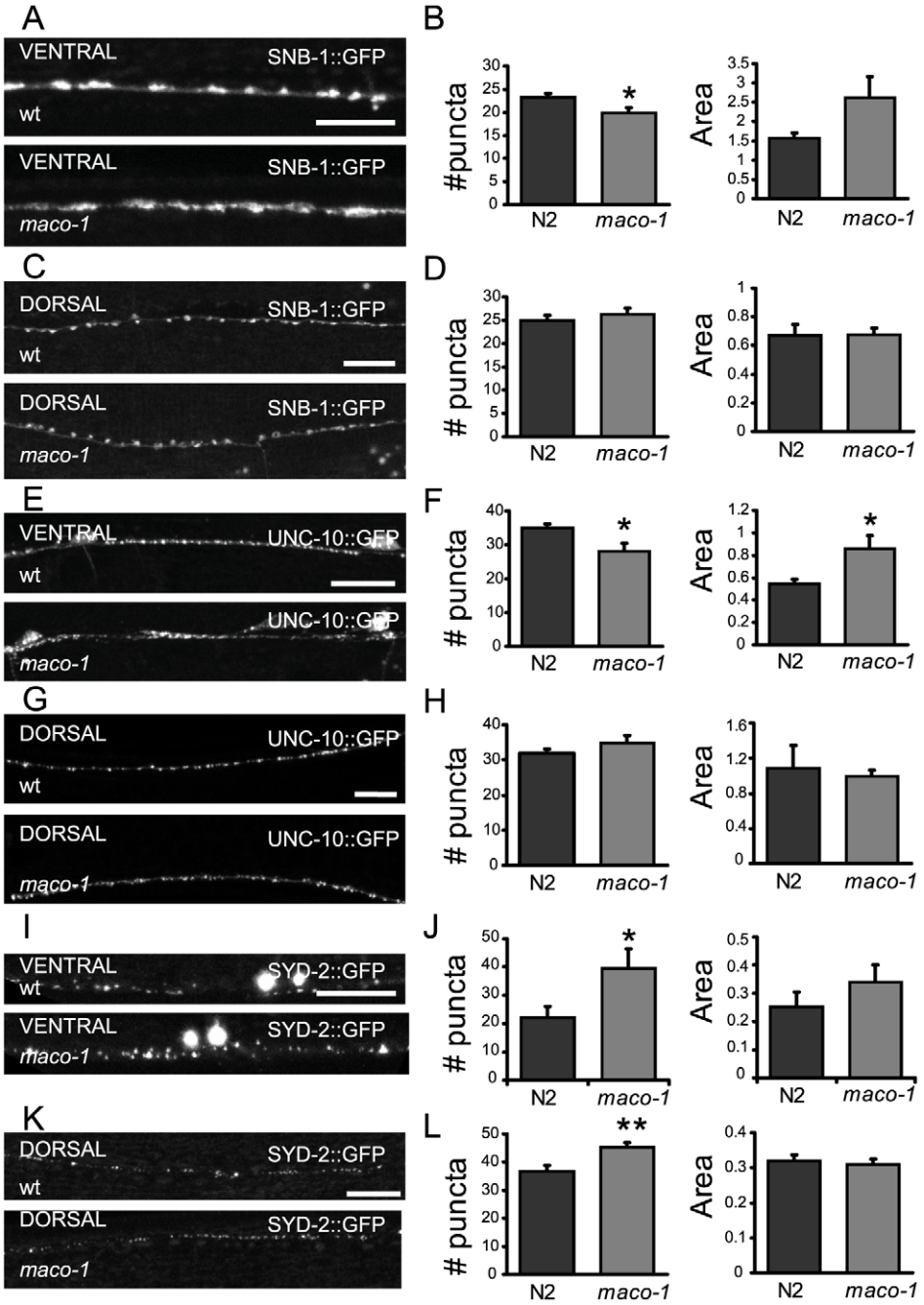

Figure 6. *maco-1* mutants have subtle synaptic morphology defects. SNB-1::GFP puncta along the ventral (A) and dorsal (C) nerve cords of wild type and *maco-1(db9)* mutants. (B, D) Quantification of SNB-1::GFP puncta number and area in wild type and *maco-1* mutants in ventral (B) and dorsal (D) cords. (E, G) UNC-10::GFP puncta along the ventral (E) and dorsal (G) nerve cords of wild type and *maco-1(db9)* mutants. (F, H) Quantification of UNC-10::GFP puncta number and area in wild type and *maco-1* mutants in ventral (F) and dorsal (H) cords. (I, K) SYD-2::GFP puncta in the ventral (I) and dorsal (K) nerve cords of wild type and *maco-1* mutants. (J, L) Quantification of SYD-2::GFP puncta number and area in the ventral (J) and dorsal (L) cords of wild type and *maco-1* mutants. The transgenic arrays used are: SNB-1::GFP (*juIs1*), SYD-2::GFP (*hpIs3*) and UNC-10::GFP (*hpIs61*). Puncta analysis focussed on a 100 μm interval between motorneurons VD10 and VD12. All images are of 1-day-old adult hermaphrodites. Numbers are mean ± s.e.m. Scale bar, 10 μm. * $p<0.05$, ** $p<0.01$.
doi:10.1371/journal.pgen.1001341.g006

Discussion

Macoilins are a conserved family of multipass transmembrane proteins whose function has been mysterious. Members of the family can be found in eukaryotes that have a recognizable nervous system, from placozoa to humans, but not in yeast or *Dictyostelium*. Macoilins are expressed broadly but specifically in the nervous system. *C. elegans* macoilin is absent from neurites and is localized to the RER suggesting that it is involved in folding, assembly, or traffic of secreted or transmembrane proteins. The structure of macoilin contains two conserved regions: an N-terminal part that includes multiple transmembrane domains, and

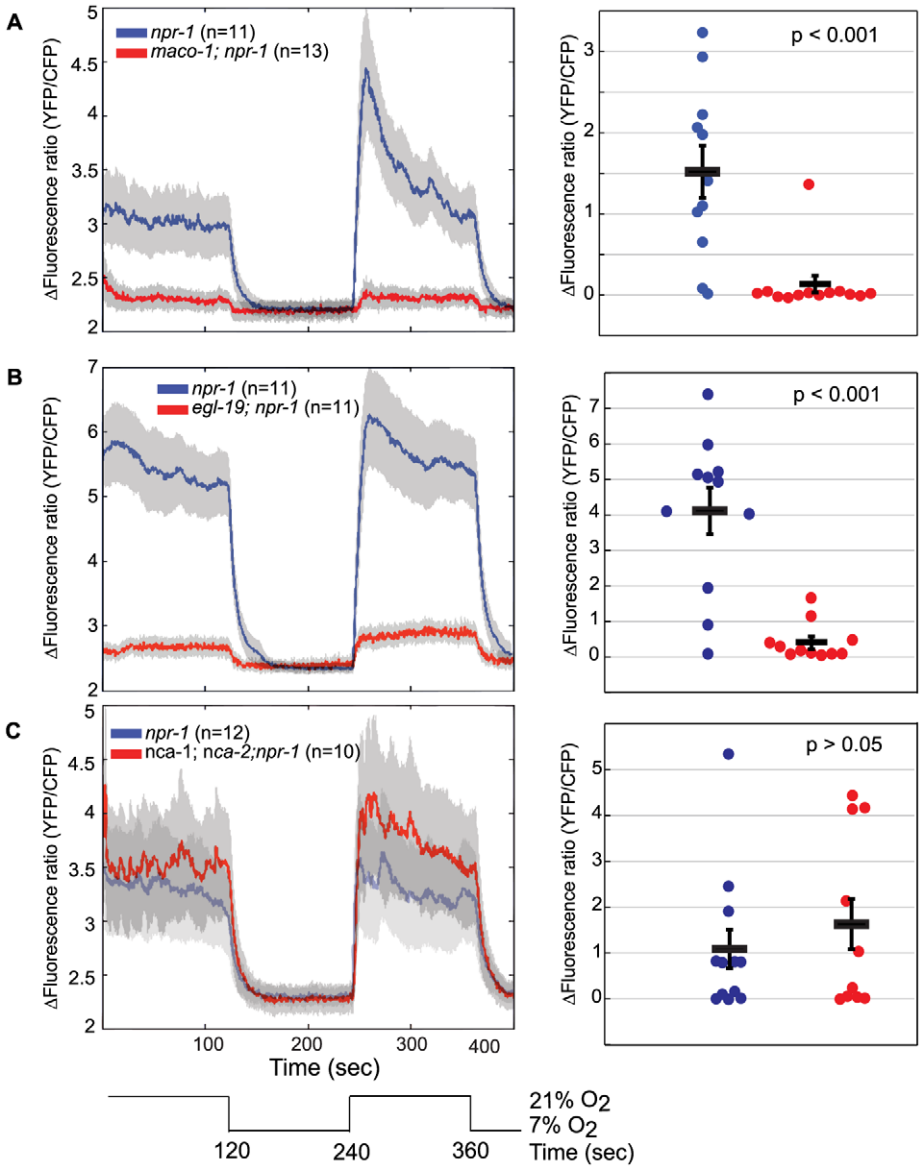

Figure 7. Loss of MACO-1 causes failure of Ca^{2+} transients in O_2-sensing neurons. Average traces and scatter plots of Ca^{2+} transients in PQR neurons responding to a 21 – 7 – 21 – 7% O_2 cycle as measured by cameleon YC3.60. (A) *maco-1 (db9); npr-1 (ad609)* worms (n = 13) usually fail to respond to O_2 changes, as opposed to *npr-1 (ad609)* worms which respond consistently (n = 11; p<0.001). (B) *egl-19(ad1006); npr-1 (ad609)* worms (n = 11) are also unresponsive to O_2, as compared with *npr-1 (ad609)* worms (n = 11; $p<0.001$). (C) *nca-1 (gk9); nca-2 (gk5); npr-1(ad609)* worms (n = 10) do not significantly ($p>0.05$) differ in their responses from *npr-1(ad609)* worms (n = 12). Gray error bars represent s.e.m. The data in Panel C were obtained on a different imaging set-up from those in panels A and B, and so cannot be directly compared.
doi:10.1371/journal.pgen.1001341.g007

a C-terminal region that has coiled coil domains; the transmembrane domains are the most highly conserved parts of the protein. This combination of structural motifs is reminiscent of that of RIC-3 and its orthologues, which are implicated in assembly and traffic of nicotinic acetylcholine receptors in *C. elegans* [45] and of nicotinic acetylcholine receptors and 5-HT3 receptors in vertebrates [46–47]. Like macoilin, RIC-3 is expressed broadly in the nervous system and is an ER membrane protein with a coiled-coil region towards the C-terminus. Macoilin mutants exhibit defects in cell intrinsic neuronal excitability, not only in PQR (this study) but also in other neurons (see associated paper by Miyara et al.). Previous work has reported that neural activity levels regulate the morphology of certain synaptic connections in *C. elegans* [33]; the synaptic morphology defects of *maco-1* mutants could therefore reflect loss of neuronal excitability. A simple hypothesis is that macoilin acts in the endoplasmic reticulum of neurons to promote the folding, assembly, or traffic of ion channels or ion channel regulators that control excitability of neurons. What might these targets be? Since baseline Ca^{2+} levels are normal in *maco-1* mutants we do not think loss of macoilin disrupts function of ion pumps that keep neurons hyperpolarized. Instead our data point towards compromised signal transduction or signal amplification downstream of the GCY-35/GCY-36 O_2-sensing soluble guanylate cyclases. As far as we can tell the cGMP-gated ion channel that transduces the O_2-evoked cGMP rise in PQR, and which includes the TAX-4 α subunit, is appropriately expressed and localized in *maco-1* mutants, although we cannot exclude the possibility that its function is somehow compromised. cGMP channels are expressed

in only a small subset of *C. elegans* neurons [48] and some of these are clearly functional in *maco-1* mutants (e.g. AWC); by contrast MACO-1 is expressed throughout the nervous system, not only in *C. elegans* but also in mouse.

The L-type VGCC α1 subunit EGL-19 is also required for O_2-evoked responses in PQR, and is expressed widely both in the nervous system and in muscle (this work; [44]. Loss-of-function mutants of *egl-19* have much more severe phenotypes than *maco-1* mutants: *egl-19(null)* mutants die as embryos. This discrepancy in phenotype makes it unlikely that MACO-1 is critical for function of all EGL-19 containing channels. Consistent with this, mutations in *maco-1* do not appear to disrupt localization of GFP- EGL-19 either in muscle or in neurons. However it remains possible that MACO-1 regulates assembly of particular subtypes of EGL-19–containing channels. L-type VGCC are composed of multiple subunits and it is the precise combination of subunits that determines the channel's regulatory properties; additionally *egl-19* mRNA itself is alternatively spliced close to its C-terminus, in a region implicated in Ca^{2+} feedback regulation [49]. An alternative scenario is that MACO-1 regulates an as yet undiscovered pathway that helps amplify the depolarization initiated by cGMP-gated ion channel activation. Identifying proteins that interact with macoilin or mutants that recapitulate the *maco-1* phenotypes will allow these hypotheses to be tested to help further unravel the function of this novel family of nervous system proteins.

Materials and Methods

Genetics

Strains used were maintained as described previously [50] and are listed in Text S1). *db1* and *db9* were isolated as suppressors of aggregation from a screen of 20,000 haploid genomes; details of the screen will be described elsewhere. *db129* was isolated in a non-complementation screen using the *db1* allele. The *db1* mutation was mapped to a 30 kb interval at the centre of Chromosome I between the SNP markers in cosmids F48A9 and D2092 using a combination of three-factor mapping and SNP genotyping [51].

Sequence mining and phylogenetics

PSI-Blast was used to search for Macoilin protein sequences, using human Macoilin as probe, at the NCBI (www.ncbi.nlm.nih.gov), Joint Genome Institute (www.jgi.doe.gov), ENSEMBL (www.ensembl.org), and the Sanger Institute (www.sanger.ac.uk). From approximately 100 sequences retrieved (e-value $>$ e-10), a subset was obtained after removing splice variants, and redundant sequences. The amino acid sequences were aligned using various programs run under the umbrella of the M-Coffee server [52]. The multiple alignment was visually inspected and curated using BioEdit [53] (Figure S10). Un-rooted phylogenetic trees were generated using a Neighbour-Joining method [54]; the robustness of the nodes was verified with 10000 bootstrap replicates using the program Phylo-Win [55].

Molecular biology

The cDNA sequence of *maco-1* was obtained by sequencing clone yk1296a05 from the Kohara collection and by using RT-PCR. Briefly, N2 mixed stage animals were extracted with Trizol, and 1–5 µg of purified total RNA reverse transcribed using an oligo-d(T) primer and SUPER RTase at 42 °C for 1 h. Primers specific for *maco-1* exons and the SL1 spliced leader sequence were used to amplify *maco-1* cDNA, and the PCR products sequenced. The *maco-1* expression construct was generated using the Gateway system (Invitrogen) [56]. The Destination vector included 4 kb of the sequence upstream of the *maco-1* start site but omitted 318 bp between the trans-splice site and the initiation codon. The Entry vector places *maco-1* cDNA plus 9 bp of the sequence upstream in an artificial operon with gfp [34]. This construct was sequenced and injected at 50 ng/µl with *lin-15*(+) as the co-injection marker.

Transgenic rescue: The fosmid WRM0640bE08, containing D2092.5, was injected into the strain AX129, *maco-1(db9);npr-1(ad609)* at a concentration of 2 ng/µl, with 50 ng/µl of *punc-122::gfp* as a co-injection marker. Further transgenic rescue experiments were carried out using a PCR amplified genomic DNA fragment containing the D2092.5 gene, including 4 kb upstream of the initiation codon and 1 kb after the stop codon. This PCR product was injected into the AX59, *maco-1(db9); npr-1(ad609)* strain at a concentration of 2 ng/µl, using *pmyo-2::gfp* as a co-injection marker (4 ng/µl) and 1 kb-ladder (96 ng/µl) as carrier.

Sub-cellular markers (a kind gift of Melissa M. Rolls, Penn State University) were used as described [4]. The plasmids used were C24F3.1a (*pglr-1::yfp-TRAM*), Y46G5a.5 (*pglr-1::yfp-PIS*), F55-8H1.1 (*pglr-1::yfp-MANS*) and M01D7.6 (*pglr-1::yfp-EMERIN*). These plasmids were individually injected at 4 ng/µl into AX206, *lin-15(n765ts)* animals with a *lin-15*(+) co-injection marker (40 ng/µl). All primer sequences used are available upon request.

The *pgcy-32::tax-4-gfp* transgene was made using Gateway; *tax-4* cDNA was tagged at the 3'end with gfp and injected (at 10 ng/ul) with a *lin-15(+)* co-injection marker (40 ng/ul) into *npr-1(ad609) lin-15(n765ts)* animals. A fosmid containing the full-length *egl-19* gene was modified by recombineering so as to express N-terminally GFP tagged EGL-19 from its endogenous control sequences. The recombineered fosmid was co-injected at 5 ng /ul with a *pgcy-32::mcherry* co-injection marker (25 ng/ul) and carrier DNA (DNA ladder at 70 ng/ul).

Immunostainings

Mix-staged worms were stained following the modified Ruvkun and Finney method [57]. Primary antibodies were used at dilutions of 1/50 and 1/500 for mouse monoclonal anti-GFP antibody (clones 7.1 and 13.1; Roche, Germany) and rabbit polyclonal anti-MCL, respectively. Antibodies were incubated at 4 °C for 16 hrs with gentle mixing. The secondary antibodies Alexa Fluor 546 nm goat anti-rat IgG (H+L) (Invitrogen, UK) and AlexaFluor 488 nm goat anti-mouse (Invitrogen, UK) were used at a final dilution of 1/500 (4 mg/ml) and 1/250 (10 mg/ml), respectively; DAPI was added to a final concentration of 5 mM. After an incubation of 2 hrs at room temperature, worms were thoroughly washed with AbB Buffer (the details of buffer composition can be found in the Text S1), mounted in agarose and imaged.

Fluorescent microscopy and quantification

Live animals were anaesthetized with 10 mM sodium azide, mounted on 2 % agarose pads, and examined under epifluorescence using a Zeiss Axioskop fluorescent microscope. Confocal images were taken using a Radiance Plus Confocal Scanning System (Bio-Rad). The images were processed and analyzed with LaserSharp2000 software (Bio-Rad). The different GFP markers were visualized in the different backgrounds as described previously [29],[58]. Measurements of GFP puncta were performed on confocal images. Briefly, confocal images were projected into a single plane using the maximum projection method and exported as a tiff file with a scale bar. Fluorescence intensity, number of puncta, total fluorescence and punctum area were measured in ImageJ. These numbers were exported to

Microsoft Excel for statistical analyses using Student's two-tailed t-test.

Behavioral and pharmacological assays

Aggregation assays were done as previously described [14]. Egg-laying assays followed [59] with the following modifications. Worms were synchronized and young adults picked to unseeded plates to remove adhering food before transfer to plates seeded with 50 µl of *E. coli* OP50 or to un-seeded plates. Rings of 100 µl of 4M D-Fructose were painted on no-food plates to trap animals. Worms were left for one hour, then removed and eggs counted. Plates in which worms could not be found were discarded (around 10% in plates without food). Harsh touch was assayed by poking animals with a platinum wire pick. To analyze swimming defects, single worms were transferred to M9 media and left to equilibrate for a minute; head swings were counted during 10 second intervals; for coiling we counted the number of times the worm's nose touched the mid body in one minute. The results of the behavioral assays were analyzed using a two-tailed *t*-test. Aldicarb and levamisole assays were done as described [25]. Briefly, sensitivity to 1 mM aldicarb (Chem Services) or 0.4 mM levamisole was determined by assaying the time course of the onset of paralysis following acute exposure of a population of animals to these drugs. In each experiment, 25 worms were placed on drug plates and prodded every 10 min over a 2 h period to determine if they retained the ability to move. Worms that failed to respond at all to the harsh touch were classified as paralyzed. Each experiment was repeated five times.

Ca^{2+} imaging

Ca^{2+} responses of PQR neurons to O_2 stimuli were imaged as described previously (Persson et al 2009) on an inverted microscope (Axiovert, Zeiss), using a 40× C Apochromat lens and Metamorph acquisition software (Molecular Devices). To measure Ca^{2+} we used the ratiometric FRET sensor YC3.60 [35]. Briefly, worms were glued to agarose pads using Nexaband glue (WPI Inc) and placed under the stem of a Y-chamber microfluidic device. Photobleaching was limited by using a 2.0 optical-density filter and a shutter to limit exposure time to 100 ms per frame. An excitation filter (Chroma) restricted illumination to the cyan channel. A beam splitter (Optical Insights) was used to seperate the cyan and yellow emission light. The ratio of the background-subtracted fluorescence in the CFP and YFP channels was calculated with Jmalyze [60]. Fluorescence ratio (YFP/CFP) plots and measurements of mean baseline ratios and mean peak ratios were made in Matlab (The MathWorks). Movies were captured at 2 frames per second. Average Ca^{2+} traces were compiled from at least six recordings per condition made across two or more days.

Statistics

Whenever the data fitted a normal distribution ($p<0.05$, Kolmogorov-Smirnov) a two-sample (unranked) *t*-test was used. For non-normally distributed data, the non-parametric Kolmogorov-Smirnov (K-S) -test was used.

Supporting Information

Figure S1 *maco-1* mutants exhibit robust attraction to AWA and AWC-sensed odors, and strong avoidance of high osmotic tension. (A) *maco-1(db1); npr-1(ad609)* and *maco-1(db9); npr-1(ad609)* mutants chemotax strongly to a 1/1000 dilution of diacetyl, an odor detected by the AWA neurons, and (B) a 1/200 dilution of benzaldehyde, an odor detected by AWC neurons. N2 and *npr-1(ad609)* animals are shown as positive controls. *osm-9(ky10)* mutants are defective in a TRPV like channel required in AWA for diacetyl sensing; *tax-4(p678)* mutants are defective in a cGMP-gated ion channel required in AWC for benzaldehyde responses. For A and B each bar represents the average of 4 assays. (C) *maco-1* worms exhibit strong avoidance of regions with high osmotic tension. Each data point represents the average response of at least 400 animals in 40 assays. For all panels error bars indicate s.e.m. (D) *maco-1(db9)* mutants do not aggregate or border. (E, F) The *maco-1* locomotory defects increase with age. Shown are number of head swings made per second by swimming animals the first and fourth day of adulthood (E). (F) Plots the ratio of head swings on day 1 compared to day 4 for swimming *npr-1* and *maco-1; npr-1* animals. (G) *maco-1(db9); npr-1(ad609)* and *maco-1(db9)/qDf16; npr-1(ad609)* animals have similar phenotypes. Shown is the reversal frequency after harsh touch as a percentage of the response of *npr-1(ad609)* animals.
Found at: doi:10.1371/journal.pgen.1001341.s001 (0.26 MB PDF)

Figure S2 The D2092.5 gene rescues *maco-1* associated phenotypes. (A) Aggregation and bordering deficits of *maco-1(db9); npr-1(ad609)* animals are substantially but not completely rescued by a fosmid containing D2092.5, as well as by a PCR fragment spanning the D2092.5 gene. The graph compares the behavior of animals bearing the transgene, as indicated by the GFP co-injection marker, and those that do not (n = 3; *D*-test). The co-injection markers are *myo-2::GFP* (for the PCR fragment) and *unc-122::GFP* (for the fosmid). (B) A PCR product spanning the D2092.5 gene suppresses the excessive reversals of *maco-1(db9); npr-1(ad609)* animals induced by a harsh prod (n = 28–30; *t*-test). (C) A fosmid containing D2092.5 partially rescues the swimming defects of *maco-1(db9); npr-1(ad609)* animals (n = 40–70; D-test). (D) A PCR product spanning the D2092.5 gene restores suppression of egg-laying in *maco-1(db9); npr-1* animals when food is absent (n = 23–28). * equals $p<0.05$; ** equals $p<0.01$; *** equals $p<0.001$. Errors indicate s.e.m.
Found at: doi:10.1371/journal.pgen.1001341.s002 (0.66 MB PDF)

Figure S3 *maco-1* is expressed in neurons from early stages. Confocal projections of worms transgenic for *pmaco-1*::*maco-1*::gfp, an operon that expresses soluble GFP in tandem with MACO-1. (A) Early developmental stages and (B) adult worms. Time indicates approximate number of hours after first division. Scale bars represent (A) 10 and (B) 40 µm.
Found at: doi:10.1371/journal.pgen.1001341.s003 (4.07 MB PDF)

Figure S4 Endogenous MACO-1 is localized in the cell body of neurons. Immunohistochemical staining using affinity purified anti-MACO-1 antibodies. Shown are the tail regions of (A) N2 and (B) *maco-1(db9)* adults, and (C) *maco-1(db9)* larvae. The stop codon associated with the *db9* allele truncates the epitope used to generate the anti-MACO-1 antibody. Arrowheads indicate antibody signal. Scale bars represent 20 µm.
Found at: doi:10.1371/journal.pgen.1001341.s004 (2.04 MB PDF)

Figure S5 MACO-1 is excluded from neurites and localizes to ER-like structures at embryonic stages. Embryos at (A) approximately the 100 cell stage, (B) the comma-stage, (C) the three-fold stage, and (D) a L1 larvae emerging from egg-shell stained with anti-MACO-1 polyclonal antibodies; panel D also shows DAPI staining. Scale bars represent 5 µm.
Found at: doi:10.1371/journal.pgen.1001341.s005 (1.78 MB PDF)

Figure S6 MACO-1 is an ER resident protein. Confocal optical sections showing neuronal cell bodies in worms bearing extra-chromosomal arrays that express either the YFP-tagged nuclear envelope marker emerin (A–D), or the YFP-tagged Golgi marker mannosidase (E–H), and co-stained with anti-MACO-1 antibodies

(B, F), anti-GFP antibodies (A, E) and DAPI (C, G). Arrowheads indicate co-localisation between the MACO-1 and the nuclear envelop marker. EMR, Emerin; MANS, Mannosidase. Scale bars represent 1 micron.
Found at: doi:10.1371/journal.pgen.1001341.s006 (0.41 MB PDF)

Figure S7 *C. elegans* macoilin mutants have wild-type neuronal cell morphology, axon guidance, and axon polarity (A). The morphology of cell bodies and axons of VD and DD neurons visualized using a *punc-47::gfp* transgene appears wild type in *maco-1(db9)* mutant animals. Scale bar: 20 μm. (B). The mechanosensory neurons appear wild type in *maco-1(db9)* animals. Neurons were visualized using *pmec-4::gfp*. Scale bar: 20 μm. (C) *maco-1(db9)* mutants do not have any apparent defect in the morphology of sensory cilia, dendrites, cell bodies and axons of ADL neurons, as visualized using a *psrh-220::gfp* marker. Scale bar: 10 μm. (D, E) *punc-25*::SNB-1::GFP is localized along the ventral processes of the DD neurons in N2 wild type and *maco-1* L1 larvae. Polarity of DD neurons in *maco-1* L1 worms is normal, and MACO-1 is not essential for transport of synaptic vesicles to synapses (see also Figure 6). Scale bar: 20 μm. (F, G) In both *npr-1(ad609)* and *maco-1(db9); npr-1(ad609)* animals SNB-1::GFP is localized along the axonal processes in URX neurons, as predicted by the electron micrograph reconstruction of this neuron. The transgene used is *pgcy-36::snb-1-YFP*. Scale bar: 10 μm.
Found at: doi:10.1371/journal.pgen.1001341.s007 (4.57 MB PDF)

Figure S8 Localization of TAX-4-GFP appears wild type in *maco-1* mutants. Localization of TAX-4::GFP appears wild-type in *maco-1* mutants. *npr-1(ad609)* (A–B) and *maco-1(db9); npr-1(ad609)* (C–F) worms expressing *pgcy-32::tax-4::GFP* from extrachromosomal arrays. TAX-4 can be observed in URX cell bodies (arrow head) and dendrites (arrows) in both *npr-1(ad609)* and *maco-1(db9); npr-1(ad609)* animals (A–D). TAX-4::GFP traffics correctly to PQR dendrites in *maco-1(db9); npr-1(ad609)* worms (E–F). Scale bars represent 10 microns (A, C, E) and 2 microns (B, D, F).
Found at: doi:10.1371/journal.pgen.1001341.s008 (1.04 MB PDF)

Figure S9 Loss of *maco-1* does not cause obvious defects to localization of GFP-EGL-19. *maco-1* mutants do not have altered subcellular localization of GFP::EGL-19. *npr-1(ad609)* (A, C, E) and *maco-1; npr-1(ad609)* (B, D, F) worms expressing GFP::EGL-19. In both *npr-1(ad609)* and *maco-1(db9);npr-1(ad609)* animals GFP::EGL-19 can be mainly found in the cell bodies of neurons, in the head (A and B) and tail (C and D) regions. No conspicuous differences in GFP::EGL-19 localization are observed between the motorneuron cell bodies of *npr-1(ad609)* and *maco-1(db9);npr-1(ad609)* worms (E and F). In both *npr-1(ad609)* (data not shown) and *maco-1(db9);npr-1(ad609)* worms, GFP:EGL-19 was restricted to cell bodies in neurons of the ventral cord (G). Scale bars represent 20 microns (A, B, C, D, G) and 2 microns (E, F). In panels A – D red indicates fluorescence from the co-injection marker, *pgcy-32::mcherry*, which directs expression in the URX and AQR head neurons and the PQR tail neuron. Co-localization between red and green fluorescence confirms that EGL-19 is expressed in AQR, PQR and URX neurons.
Found at: doi:10.1371/journal.pgen.1001341.s010 (1.97 MB PDF)

Figure S10 MACO-1 homologues are present in many eumetazoan lineages. Multiple alignment of retrieved sequences of MACO-1 homologues. Black and gray shadings indicate a minimum of 70% sequence identity and similarity, respectively.
Found at: doi:10.1371/journal.pgen.1001341.s009 (0.06 MB PDF)

Text S1 Supporting materials and methods.
Found at: doi:10.1371/journal.pgen.1001341.s011 (0.04 MB DOC)

Acknowledgments

We thank Akiko Miyara and Ikue Mori for sharing unpublished data; Melissa Rolls for plasmids; Yuji Kohara for cDNAs; Colin Dolphin for help with recombineering; Emanuel Busch, Eiji Kodama, Patrick Laurent, Zoltan Soltesz, and Kate Weber for critical reading of the manuscript. We gratefully acknowledge receipt of strains from the *Caenorhabditis* Genetics Center, Mei Zhen, Erik Jorgensen, and Yishi Jin. LBR thanks Dr. Jean-Louis Bessereau for his support.

Author Contributions

Conceived and designed the experiments: FAC LBR AC MdB. Performed the experiments: FAC LBR AC MdB. Analyzed the data: FAC LBR AC MdB. Contributed reagents/materials/analysis tools: BHHC ML. Wrote the paper: FAC LBR MdB.

References

1. Almedom RB, Liewald JF, Hernando G, Schultheis C, Rayes D, et al. (2009) An ER-resident membrane protein complex regulates nicotinic acetylcholine receptor subunit composition at the synapse. EMBO J 28: 2636–2649.
2. Vogel F, Hartmann E, D G, Rapoport TA (1990) Segregation of the signal sequence receptor protein in the rough endoplasmic reticulum membrane. Eur J Cell Biol 53: 197–202.
3. Meyer HA, Grau H, Kraft R, Kostka S, Prehn S, et al. (2000) Mammalian Sec61 is associated with Sec62 and Sec63. J Biol Chem 275: 14550–14557.
4. Rolls MM, Hall DH, Victor M, Stelzer EH, Rapoport TA (2002) Targeting of rough endoplasmic reticulum membrane proteins and ribosomes in invertebrate neurons. Mol Biol Cell 13: 1778–1791.
5. Srivastava M, Begovic E, Chapman J, Putnam NH, Hellsten U, et al. (2008) The *Trichoplax* genome and the nature of placozoans. Nature 454: 955–960.
6. Chapman JA, Kirkness EF, Simakov O, Hampson SE, Mitros T, et al. (2010) The dynamic genome of *Hydra*. Nature 464: 592–596.
7. Cameron RA, Samanta M, Yuan A, He D, Davidson E (2009) SpBase: the sea urchin genome database and web site. Nucleic Acids Res 37: D750–4.
8. Lander ES, Linton LM, Birren B, Nusbaum C, Zody MC, et al. (2001) Initial sequencing and analysis of the human genome. Nature 409: 860–921.
9. Venkatachalam K, Montell C (2007) TRP channels. Annu Rev Biochem 76: 387–417.
10. O'Donnell M, Chance RK, Bashaw GJ (2009) Axon growth and guidance: receptor regulation and signal transduction. Annu Rev Neurosci 32: 383–412.
11. Brose N, Rosenmund C, Rettig J (2000) Regulation of transmitter release by Unc-13 and its homologues. Curr Opin Neurobiol 10: 303–311.
12. Sudhof TC (2004) The synaptic vesicle cycle. Annu Rev Neurosci 27: 509–547.
13. Kuvbachieva A, Bestel AM, Tissir F, Maloum I, Guimiot F, et al. (2004) Identification of a novel brain-specific and Reelin-regulated gene that encodes a protein colocalized with synapsin. Eur J Neurosci 20: 603–610.
14. de Bono M, Bargmann CI (1998) Natural variation in a neuropeptide Y receptor homolog modifies social behavior and food response in *C. elegans*. Cell 94: 679–689.
15. Persson A, Gross E, Laurent P, Busch KE, Bretes H, et al. (2009) Natural variation in a neural globin tunes oxygen sensing in wild *Caenorhabditis elegans*. Nature 458: 1030–1033.
16. Rogers C, Reale V, Kim K, Chatwin H, Li C, et al. (2003) Inhibition of *Caenorhabditis elegans* social feeding by FMRFamide-related peptide activation of NPR-1. Nat Neurosci 6: 1178–1185.
17. Cheung BH, Cohen M, Rogers C, Albayram O, de Bono M (2005) Experience-dependent modulation of *C. elegans* behavior by ambient oxygen. Curr Biol 15: 905–917.
18. Bargmann CI, Hartwieg E, Horvitz HR (1993) Odorant-selective genes and neurons mediate olfaction in *C. elegans*. Cell 74: 515–527.
19. Bargmann CI, Thomas JH, Horvitz HR (1990) Chemosensory cell function in the behavior and development of *Caenorhabditis elegans*. Cold Spring Harb Symp Quant Biol 55: 529–538.
20. Miller KG, Alfonso A, Nguyen M, Crowell JA, Johnson CD, et al. (1996) A genetic selection for *Caenorhabditis elegans* synaptic transmission mutants. Proc Natl Acad Sci U S A 93: 12593–12598.
21. Waggoner LE, Hardaker LA, Golik S, Schafer WR (2000) Effect of a neuropeptide gene on behavioral states in *Caenorhabditis elegans* egg-laying. Genetics 154: 1181–1192.

22. Kumada M, Iwamoto S, Kamesaki T, Okuda H, Kajii E (2002) Entire sequence of a mouse chromosomal segment containing the gene Rhced and a comparative analysis of the homologous human sequence. Gene 299: 165–172.
23. Hall DH, Hedgecock EM (1991) Kinesin-related gene *unc-104* is required for axonal transport of synaptic vesicles in *C. elegans*. Cell 65: 837–847.
24. Byrd DT, Kawasaki M, Walcoff M, Hisamoto N, Matsumoto K, et al. (2001) UNC-16, a JNK-signaling scaffold protein, regulates vesicle transport in *C. elegans*. Neuron 32: 787–800.
25. Nurrish S, Segalat L, Kaplan JM (1999) Serotonin inhibition of synaptic transmission: $G_{\alpha o}$ decreases the abundance of UNC-13 at release sites. Neuron 24: 231–242.
26. Loria PM, Hodgkin J, Hobert O (2004) A conserved postsynaptic transmembrane protein affecting neuromuscular signaling in *Caenorhabditis elegans*. J Neurosci 24: 2191–2201.
27. White JG, Southgate E, Thomson JN, Brenner S (1986) The structure of the nervous system of the nematode *Caenorhabditis elegans*. Philosophical Transactions of the Royal Society of London B. pp 1–340.
28. Hallam SJ, Jin Y (1998) *lin-14* regulates the timing of synaptic remodelling in *Caenorhabditis elegans*. Nature 395: 78–82.
29. Yeh E, Kawano T, Weimer RM, Bessereau JL, Zhen M (2005) Identification of genes involved in synaptogenesis using a fluorescent active zone marker in *Caenorhabditis elegans*. J Neurosci 25: 3833–3841.
30. Deken SL, Vincent R, Hadwiger G, Liu Q, Wang ZW, et al. (2005) Redundant localization mechanisms of RIM and ELKS in *Caenorhabditis elegans*. J Neurosci 25: 5975–5983.
31. Zhen M, Huang X, Bamber B, Jin Y (2000) Regulation of presynaptic terminal organization by *C. elegans* RPM-1, a putative guanine nucleotide exchanger with a RING-H2 finger domain. Neuron 26: 331–343.
32. Sone M, Suzuki E, Hoshino M, Hou D, Kuromi H, et al. (2000) Synaptic development is controlled in the periactive zones of *Drosophila* synapses. Development 127: 4157–4168.
33. Zhao H, Nonet ML (2000) A retrograde signal is involved in activity-dependent remodeling at a *C. elegans* neuromuscular junction. Development 127: 1253–1266.
34. Coates JC, de Bono M (2002) Antagonistic pathways in neurons exposed to body fluid regulate social feeding in *Caenorhabditis elegans*. Nature 419: 925–929.
35. Nagai T, Yamada S, Tominaga T, Ichikawa M, Miyawaki A (2004) Expanded dynamic range of fluorescent indicators for Ca(2+) by circularly permuted yellow fluorescent proteins. Proc Natl Acad Sci U S A 101: 10554–10559.
36. Gray JM, Karow DS, Lu H, Chang AJ, Chang JS, et al. (2004) Oxygen sensation and social feeding mediated by a *C. elegans* guanylate cyclase homologue. Nature 430: 317–322.
37. Cheung BH, Arellano-Carbajal F, Rybicki I, De Bono M (2004) Soluble Guanylate Cyclases Act in Neurons Exposed to the Body Fluid to Promote *C. elegans* Aggregation Behavior. Curr Biol 14: 1105–1111.
38. Yeh E, Ng S, Zhang M, Bouhours M, Wang Y, et al. (2008) A putative cation channel, NCA-1, and a novel protein, UNC-80, transmit neuronal activity in *C. elegans*. PLoS Biol 6: e55. doi:10.1371/journal.pbio.0060055.
39. Hilliard MA, Apicella AJ, Kerr R, Suzuki H, Bazzicalupo P, et al. (2004) In vivo imaging of *C. elegans* ASH neurons: cellular response and adaptation to chemical repellents. Embo J.
40. Jeziorski MC, Greenberg RM, Anderson PA (2000) The molecular biology of invertebrate voltage-gated Ca(2+) channels. J Exp Biol 203: 841–856.
41. Schafer WR, Kenyon CJ (1995) A calcium-channel homologue required for adaptation to dopamine and serotonin in *Caenorhabditis elegans*. Nature 375: 73–78.
42. Shtonda B, Avery L (2005) CCA-1, EGL-19 and EXP-2 currents shape action potentials in the *Caenorhabditis elegans* pharynx. J Exp Biol 208: 2177–2190.
43. Catterall WA, Perez-Reyes E, Snutch TP, Striessnig J (2005) International Union of Pharmacology. XLVIII. Nomenclature and structure-function relationships of voltage-gated calcium channels. Pharmacol Rev 57: 411–425.
44. Kim H, Pierce-Shimomura JT, Oh HJ, Johnson BE, Goodman MB, et al. (2009) The dystrophin complex controls bk channel localization and muscle activity in *Caenorhabditis elegans*. PLoS Genet 5: e1000780. doi:10.1371/journal.pgen.1000780.
45. Halevi S, McKay J, Palfreyman M, Yassin L, Eshel M, et al. (2002) The *C. elegans ric-3* gene is required for maturation of nicotinic acetylcholine receptors. EMBO J 21: 1012–1020.
46. Wang Y, Yao Y, Tang XQ, Wang ZZ (2009) Mouse RIC-3, an endoplasmic reticulum chaperone, promotes assembly of the alpha7 acetylcholine receptor through a cytoplasmic coiled-coil domain. J Neurosci 29: 12625–12635.
47. Castillo M, Mulet J, Gutierrez LM, Ortiz JA, Castelan F, et al. (2006) Role of the RIC-3 protein in trafficking of serotonin and nicotinic acetylcholine receptors. J Mol Neurosci 30: 153–156.
48. Coburn CM, Bargmann CI (1996) A putative cyclic nucleotide-gated channel is required for sensory development and function in *C. elegans*. Neuron 17: 695–706.
49. Dolphin AC (2009) Calcium channel diversity: multiple roles of calcium channel subunits. Curr Opin Neurobiol 19: 237–244.
50. Sulston J, Hodgkin J (1988) Methods. In: Wood WB, ed. The nematode *Caenorhabditis elegans*. Cold Spring Harbor: CSHL Press. pp 587–606.
51. Wicks SR, Yeh RT, Gish WR, Waterston RH, Plasterk RH (2001) Rapid gene mapping in *Caenorhabditis elegans* using a high density polymorphism map. Nat Genet 28: 160–164.
52. Moretti S, Armougom F, Wallace IM, Higgins DG, Jongeneel CV, et al. (2007) The M-Coffee web server: a meta-method for computing multiple sequence alignments by combining alternative alignment methods. Nucleic Acids Res 35: W645–8.
53. Tippmann HF (2004) Analysis for free: comparing programs for sequence analysis. Brief Bioinform 5: 82–87.
54. Saitou N, Nei M (1987) The neighbor-joining method: a new method for reconstructing phylogenetic trees. Mol Biol Evol 4: 406–425.
55. Galtier N, Gouy M, Gautier C (1996) SEAVIEW and PHYLO_WIN: two graphic tools for sequence alignment and molecular phylogeny. Comput Appl Biosci 12: 543–548.
56. Walhout AJ, Temple GF, Brasch MA, Hartley JL, Lorson MA, et al. (2000) GATEWAY recombinational cloning: application to the cloning of large numbers of open reading frames or ORFeomes. Methods Enzymol 328: 575–592.
57. Bettinger JC, Lee K, Rougvie AE (1996) Stage-specific accumulation of the terminal differentiation factor LIN-29 during *Caenorhabditis elegans* development. Development 122: 2517–2527.
58. Mohamed AM, Chin-Sang ID (2006) Characterization of loss-of-function and gain-of-function Eph receptor tyrosine kinase signaling in *C. elegans* axon targeting and cell migration. Dev Biol 290: 164–176.
59. Hart AC (2006) Behavior. WormBook 1–87.
60. Kerr RA, Schafer WR (2006) Intracellular Ca^{2+} imaging in *C. elegans*. Methods Mol Biol 351: 253–264.